Iodine-enhanced micro-CT imaging of soft tissue on the example of peripheral nerve regeneration

Patrick Heimel[1,2,3,*], Nicole Victoria Swiadek[1,3], Paul Slezak[1,3], Markus Kerbl[1,3], Sylvia Nürnberger[3,4], Heinz Redl[1,3], Andreas Herbert Teuschl[3,5], David Hercher[1,3]

1. *Ludwig Boltzmann Institute for experimental and clinical traumatology, AUVA Research center, Vienna, Austria*
2. *Karl Donath Laboratory for hard tissue and biomaterial research, Dental School Vienna, Medical University Vienna, Vienna, Austria*
3. *Austrian Cluster for Tissue Regeneration, Vienna, Austria*
4. *Department of Trauma Surgery, Medical University Vienna, Vienna, Austria*
5. *Department of Biochemical Engineering, UAS Technikum Wien, Vienna, Austria*

* Correspondence: patrick.heimel@trauma.lbg.ac.at

Abstract

Microcomputed tomography (µCT) is widely used for the study of mineralized tissues but a similar use for soft tissues is hindered by their low X-ray attenuation. This limitation can be overcome by the recent development of different staining techniques. Staining with Lugol's solution, a mixture of one part iodine and two parts potassium iodine in water stands out among these techniques for its low complexity and cost. Currently, Lugol staining is mostly used for anatomical study of tissues. In the present study we seek to optimize the quality and reproducibility of the staining for *ex vivo* visualization of soft tissues in the context of a peripheral nerve regeneration model in the rat.

We show that the staining result not only depends on the concentration of the staining solution, but also on the amount of stain in relation to the tissue volume and composition, necessitating careful adaptation of the staining to the tissue. This optimization can be simplified by a stepwise staining which we show to yield a similar result compared to staining in a single step. Lugol staining solution results in concentration dependent tissue shrinkage which can be minimized but not eliminated. We compared the shrinkage of tendon, nerve, skeletal muscle, heart, brain and kidney with six iterations of Lugol staining.

60 ml of 0.3% Lugol's solution per cm^3 of tissue for 24h yielded good results on the example of peripheral nerve regeneration model and we could show that the regenerating nerve inside a silk fibroin tube can be visualized in 3D using this staining technique. This information helps in deciding the region of interest for histological imaging and provides a 3D context to histological findings. Correlating both imaging modalities has the potential to improve the understanding of the regenerative process.

Keywords: Lugol's iodine, Radiocontrast Agents, Nerve Regeneration, X-Ray Microtomography

Introduction

Microcomputed tomography (µCT) has been used as a valuable tool for understanding and quantifying regenerative processes in bone and other mineralized tissues[1]. So far no widespread use of µCT for the evaluation of soft tissues in a similar manner is routinely used due to the low X-ray attenuation of non-mineralized tissues. To overcome this limitation of the µCT staining of soft tissue, Lugol's solution, and other staining methods were developed among others by Metcher et. al.[2,3]. The use of these staining techniques has been mostly limited to anatomical studies of a wide variety of biological specimen using a wide range of different concentrations of iodine and staining durations, depending on the type of tissue[4]. In regard to soft tissue perfusion, vascular detection in CT scans has been commonly facilitated via contrast agent perfusion. For instance by utilizing intravasal barium sulfate a distinct contrast of blood vessels is achieved[5,6], but incomplete vascular perfusion may lead to an underestimation of the vasculature[7].

The regeneration of peripheral nerve tissue is another field of regenerative medicine which could benefit from a more detailed analysis of e.g. tissue formation or tissue to graft reactions via µCT measurements. Despite growing microsurgical knowledge, the clinical success rate after peripheral nerve repair still remains below 70%[8,9]. Especially defects with a nerve tissue loss larger than 3 cm result in unsatisfying outcomes[10]. Therefore, the treatment of these critical size defects remains an ongoing challenge in peripheral nerve surgeries. In the clinical setting, autologous nerve transplantation is the gold standard for bridging nerve defects. However, the availability of donor nerves is limited and surgery induces an additional loss of function for the patient, resulting in a need for alternative biological or artificial nerve guiding structures to repair these defects[10,11]. So far none of the available guiding structures shows success rates comparable to autologous transplants. Hence there is a dire need for preclinical *in vivo* studies to further characterize and improve such nerve conduits and their effect on regeneration.

Besides functional tests, histologic imaging is an important tool for evaluation of the regenerating nerve, the respective conduit and interactions between these two structures. A known disadvantage of this method is that slide preparation requires cutting and staining of all samples, which is a destructive and time-consuming process. Therefore, we have established a fast, cost-efficient, reliable and easy-to-perform imaging method based on staining with an aqueous I_2KI solution, also known as Lugol's solution, which enables the generation of 3D images from full size nerve samples to identify specific regions of interest before sectioning. This allows reducing the number of histologic specimens that have to be produced and provides a precise selection of the most suitable region at the same time. Furthermore 3D images allow tracking of the exact route of the supplying vessels, which is important given that vascularization has a strong impact on the regeneration of the peripheral nerve[12,13].

Yu et. al.[14] developed a different technique for simultaneous visualization of blood vessels and nerve tissue. Their method, which employs a barium sulfate perfusion contrast agent to visualize blood vessels, uses Sihler staining[15], which stains the nerves and makes other soft tissue transparent for visualization of nerves. This process is very complex and takes 3 to 4 months from explanting the samples to the completed analysis. Moreover, this imaging technique can only provide 2D images. Three dimensional imaging of nerves in muscles has been shown to be possible with Sihler staining but further increases the complexity of the process and thereby the analysis time[16].

The here presented study seeks to optimize the Lugol staining process for soft tissue regeneration studies by evaluating the effect of different concentrations and a variation in sample storage times before staining. Of special interest to us is to evaluate how samples of unknown tissue composition can be stained in a consistent manner while minimizing the risk of overstaining and other negative side, effects such as shrinkage, of the staining process. For this purpose we stained mouse limbs, which are composed of many different tissues with very similar relative volumes between individuals. Finally the potential of these staining techniques to evaluate peripheral nerve regeneration is demonstrated.

Material and Methods

Staining Procedure

Lugol's solution is one part iodine and two parts potassium iodine in an aqueous solution. To produce a concentration of 0.3%, 0.1% (w/v) iodine and 0.2% (w/v) potassium iodine is dissolved in distillated water. All instances of Lugol staining performed in the course of this study were performed in distillated water and mixed according to the ratio above.

Preparation of Hind Limb, Organ and Tissue Samples

The front and hind limbs of 8 adult mice were used for stain and contrast measurements. Organ and tissue samples of one adult rat for shrinkage measurement including brain, kidney, heart, left and right tibialis, patella and achilles tendons and left and right sciatic nerves. All samples were harvested immediately after euthanaziation and fixed in 4% neutral buffered formalin and stored at 4 °C.

After 24 h, the tissue samples were thoroughly rinsed in tab water for at least 1 hour, transferred to 50% alcohol for 1 h and stored in 70% alcohol.

Preparation of Nerves in a Silk Fibroin Guidance Conduit

Male Sprague–Dawley rats (n=12, Charles River, Germany), weighing between 325 and 415 g, were used in the experiments. Standard rodent food and water were provided ad libitum. All experimental protocols were approved by the City Government of Vienna in accordance with the Austrian law (Animal Use Proposal Permission no. 406382/2015/12) and the National Institute of Health Guidelines.

In this study a silk fibroin based nerve guidance conduit (NGC) described in a previous study[17] was used. Briefly, this NGC is based on a braided tubular structure of raw *Bombyx mori* silk fibers, which has been degummed by boiling in a borate buffer solution[18]. The outside wall is then post-processed via subsequent incubations in the ternary solvent $CaCl_2/H_2O$/ethanol, formic acid and methanol. This combination of treatments results in a fusion of single fibers to a continuous layer which lead to the final favorable mechanical and topographical characteristics of the silk fibroin based NGC.

Surgical procedure - peripheral nerve injury

Rats were weighed and anesthetized using isoflurane (induction 3.5%, maintenance 2.0%, Forane®) at a flow rate of 800 mL/min. Body temperature was monitored continuously. The right lower limb was shaved and disinfected with povidone-iodine (Betaisodona; Mundipharma) at mid-thigh level. All following surgical procedures were carried out under an

operating microscope (Leica M651; Leica Microsystems). After stump preparation of the muscles, the sciatic nerve was exposed, and an 8 mm segment was excised, resulting in a 10 mm gap due to elastic retraction. A 12 mm silk fibroin conduit as described in[17], was implanted by insertion of the proximal and distal nerve stumps, which were coaptated to the conduit using Ethilon 8/0 epineurial sutures (Ethicon-Johnson and Johnson)Afterwards, the previously dissected muscles were adapted with 4/0 Vicryl® resorbable suture material. Final wound closure was done with the same suture performing intracutane stitches. Analgesic treatment was administered using 0.75 mg/kg bodyweight (BW) meloxicam (Metacam®; Boehringer Ingelheim, sid) and 1.25 mg/kg BW butorphanol (Butomidor®; Richter Pharma AG, bid) immediately prior to surgical procedure and for 2 days thereafter. After 7 weeks animals underwent perfusion.

Barium sulphate perfusion

To enable the quantification of blood vessels in the nerve graft region, all rats were perfused with a barium sulfate contrast agent to enable the quantification of blood vessels in the defect region as described in [6]. In brief, full body perfusion through the left ventricle with a mixture of heparin and saline was followed by neutral buffered formalin, PBS (phosphate buffered saline, Sigma-Aldrich, St. Louis, USA) and then the contrast agent, pre-heated to 40 °C, in a mixture of 30% barium sulphate (Micropaque, Guerbet, France) and 3% gelatin in PBS. Both the treated and untreated nerves of all rats were harvested. The nerves were kept in 4% neutral buffered formalin at 4°C for 24h. Afterwards the nerves were rinsed under flowing water for at least 1 h to remove formalin, transferred to 50% alcohol for 1 h before being stored in 70% alcohol.

Staining

Hind limb Staining

The mouse hind limbs were stained with different concentrations to determine the effect of iterative staining and to quantify any change of contrast between tissues (Figure 1). They were separated into single and double staining groups, each containing 4 left and 4 right limbs. Each hind limb was stained in 22.5 ml Lugol's solution in each staining step which was estimated to be approximately 15 ml Lugol's solution per cm^3 of tissue volume. Hind limb Step I: The double staining group was stained twice at 0.15% Lugol's solution for 72 h each. The single staining group was stained only once with 0.3% Lugol's solution. Hind limb Steps II/III: The double staining group was stained 4 times with 0.3% Lugol's solution and the single staining group was stained twice with 0.6% Lugol's solution.

Front Limb Staining

In order to determine the effect of the storage time on the final staining result mice front limbs were stained immediately after fixation/rehydration or after various different storage times (Figure 1). Therefore the front limbs were separated into a short storage and a long storage group, each containing 4 left and 4 right mouse front limbs. The front limbs were stained using 12.5 ml of a 0.3% Lugol's solution for 96 h. A 0.3% concentration was selected because it was the concentration used by Metscher et. al.[2,3] and is on the lower end of concentrations used in other studies[4] . The long storage group was stained 14 days after the short storage group. Both groups were stained a second time with 0.6% Lugol's solution for 18 days. The long storage group was stained 18 days after the short storage group. A 0.6% concentration was chosen as twice the concentration of the first iteration so that a clearly visible increase in stain in the tissue is achieved.

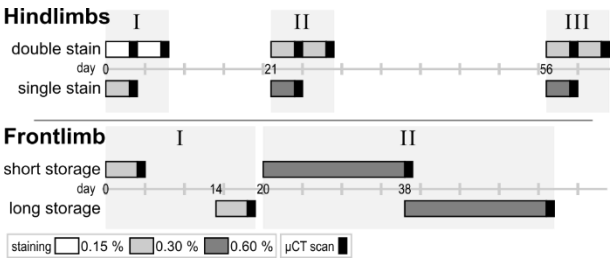

Figure 1: Staining procedure for mouse limbs: hind limbs were stained for 3 days at day 0 with 2 * 0.15% vs. 1 * 0.3% (I) and at day 21 (II) and 56 (III) with 2 * 0.3% vs 1 * 0.6%; front limbs were stained for 4 days with 0.3% at day 0 vs. day 14 (I) and for 18 days with 0.6% at day 20 vs. day 38 (II); n = 8 for all groups

After the staining duration, the iodine was almost fully absorbed by the tissue. To prevent any change to the staining by iodine being washed out, the tissues were kept in the residual staining solution. All stainings were performed at room temperature.

Nerve, Organ and Tissue Sample Staining

The organ samples were stained the same way as the double stained hind limbs using the same concentrations with 15 ml of Lugol's solution per cm^3 of tissue. Tissue volume was measured in the µCT scans of the unstained tissue and organ samples.

The nerve grafts were stained using 0.3% Lugol's solution for 48 h using approximately 60 ml Lugol's solution per cm^3 of sample. Sample volume was approximated by measuring length and diameter of the graft and the protruding nerve ends and calculating the volume of cylinders with these dimensions.

Imaging

µCT scans were performed using a SCANCO µCT 50 (SCANCO Medical AG, Brütistellen, Switzerland) specimen µCT scanner.

All limbs were scanned after each staining step with 90 kVp (200 µA, 0.5 mm Al filter, 500 projections, 300 ms integration time), at an isotropic resolution of 34.4 µm. The hind limbs were additionally scanned at an isotropic resolution of 10 µm (90 kVp, 200µA, 0.5 mm Al filter, 1000 projections, 500 ms integration time) after the final staining step.

The organ and tissue samples (except for nerve) were scanned at 45kVp before staining and 70 kVp after each staining step. 200 µA, 0.5 mm Al Filter, 500 ms integration time and 500 projections were used for all samples. Due to the different sample diameter, the resolution of the scans was different for some samples. The heart and kidney were scanned at an isotropic resolution of 34.4 µm, the tibialis muscles and the brain at 20 µm and the tendons and sciatic nerves at 10 µm.

The sciatic nerves were scanned first after harvesting and again after Lugol staining with 90 kVp (200µA, 0.5 mm Al filter, 1000 projections, 500 ms integration time), at an isotropic resolution of 7.4 µm.

Image Processing

µCT scans were exported from the µCT system as reconstructed DICOM stacks. The Stacks were loaded into Amira 6.2 (FEI Visualization Sciences Group, Mérignac, France) and each limb was registered to the first scan of that limb using the register images tool to ease in positioning of measurement regions.

Measurements

The attenuation was measured in blood, tendon and muscle tissue of the hind limb and in muscle on the front limb. Measurements were performed in the same anatomical region in the flexor digitorum brevis of the leg and the digital flexor muscles of the forelimb. (Figure 2)

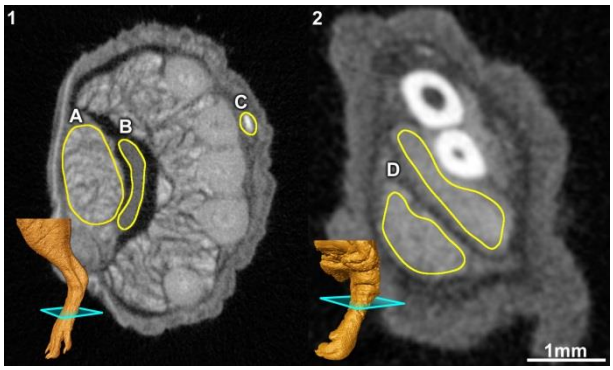

Figure 2: Region of interest (ROI) for grayscale measurements to compare the relative staining of different tissues in close proximity to one another for accurate comparisons; (1) hindlimb ROI in the flexor digitorum brevis (A), tendon (B) and blood (C); (2) forelimb ROI in the digital flexors (D); 3D image in the lower left shows the slice position

The images were imported into Fiji[19,20]and regions of interest (ROI) were drawn by hand using the lasso tool. The average grayscale values were measured in these regions. Due to the small diameter of the blood vessels in relation to the scan resolution, the average intensity is impacted by the partial volume effect[21]. To counteract this, the maximum intensity was also measured in each region, resulting in a measure of blood intensity which is less dependent on the vessel diameter.

The scans of the organ samples at different concentrations were registered to the unstained sample using DataViewer 1.5.6.2 (Bruker microCT, Kontich, Belgium). Using Fiji, the length of the organ samples were measured in four different orientations. The volume shrinkage was calculated from the measured length.

Histological verification of Nerves

After storage in 70% alcohol, dehydration was completed with further increase of a graded series of alcohol up to 100% EtOH. The nerve samples were then embedded in paraffin *via* the intermedium clearing agent xylol and sectioned at a thickness of 3–4 µm. Samples were then deparaffinized and stained with Martius yellow, Crystal red and Methyl blue (MSB), effectively staining connective tissue blue, fibrin red and erythrocytes yellow and with Luxol fast blue stain, contrasting myelin.

The histological slides were scanned using an Olympus BX61VS Virtual Slide Scanner (Olympus Corporation, Tokyo, Japan) at a resolution of 0.321 µm/pxl.

µCT scans and histological images were imported into Amira 6.2 (FEI Visualization Sciences Group, Mérignac, France). The position of the histological slide was identified in the µCT scan using a slice object. The slice was manually adjusted to correspond as close as possible to the histological slide.

Statistical Evaluation

Statistics were calculated using R 3.4.3[22,23]. Error bars in all figures denote the standard deviation. A Student's t-Test was used for significance testing with a significance level of p = 0.05.

Results

Contrast is dependent on total amount of iodine rather than concentration

When staining with a low enough concentration of Lugol's solution so that the iodine is almost completely absorbed by the tissue, the iodine is absorbed until equilibrium is reached between the absorbance capacity of the tissue and the staining solution. The small amount of staining solution (15 ml/cm^3) combined with the low concentration (0.15%-0.6%) results in almost complete absorption of iodine into the tissue. The remaining staining solution takes on a yellow translucent appearance compared to an opaque brown color beforehand. We hypothesized, that staining at multiple increments at a lower concentration would lead to a similar staining result as staining half as often with double the concentration since the amount iodine accumulated in the tissue would be the same. As shown in Figure 3 it is apparent, with the exception of blood at the highest concentration, that double staining produces a slightly lower grayscale value than single staining. The final grayscale value is very similar however, and does not result in a noticeable change in contrast between different tissues.

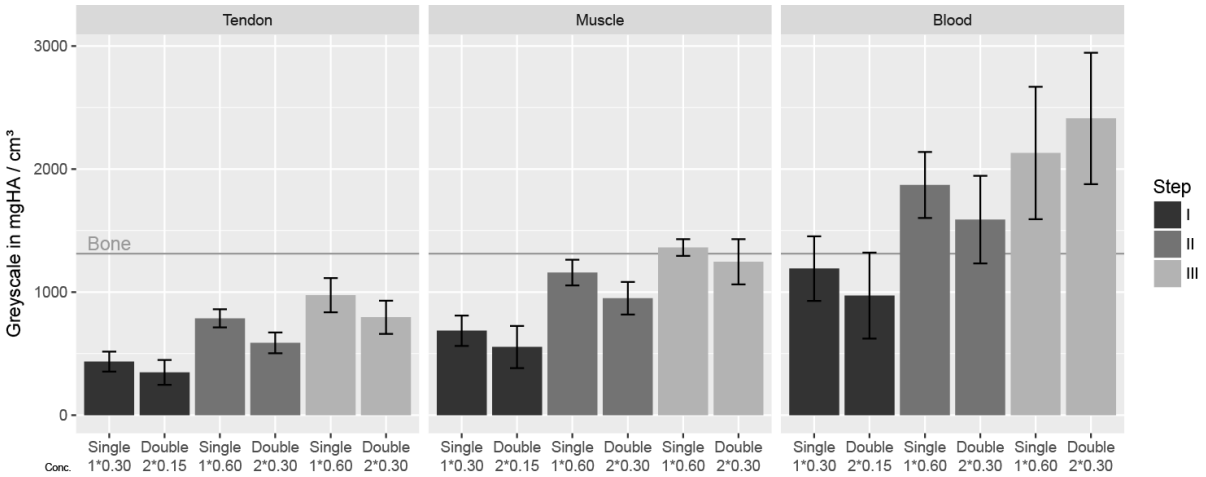

Figure 3: Comparison of greyscale value of different tissues with single vs double staining; Shown are the grayscale values of tendon, muscle and blood tissue with single and double staining with increasing amounts of iodine (I, II and III); n = 8 ±SD; The horizontal line shows the grayscale value of bone

The contrast can be measured as a ratio of greyscale values between tissue types, which remains mostly unchanged between the concentrations tested and between single and double staining (Figure 4).

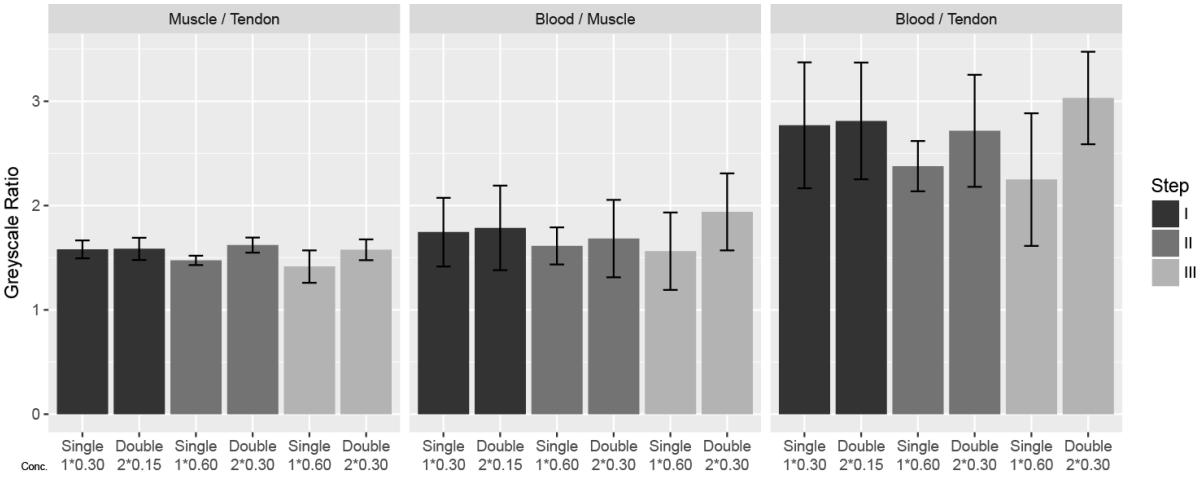

Figure 4: Contrast between tissues at different iodine concentrations with single vs double staining; Shown is the ratio of grayscale values of Muscle / Tendon, Blood / Muscle and Blood / Tendon with single and double staining with increasing amounts of iodine (I, II and III), E.g. Muscle / Tendon single staining at step I have a ratio 1.57, meaning that the muscle appears 1.57 times brighter than the tendon; n = 8 ±SD

Storage time negatively influences uptake

The influence of storage time before staining was tested in mice front limbs. No significant difference was observed in muscle tissue when storing the sample in alcohol for an additional 14 days. The front limbs immediately restained for 18 days showed an increase in grayscale value in muscle tissue while there was almost no gain in grayscale in muscle tissue in the sample stored for 18 days before restaining. A significant difference was observed in the final grayscale value in muscle tissue between short and long storage before staining (t-Test, $p = 0.033$) (Figure 5). After the initial staining, thicker parts of the limb were not fully penetrated by the stain. Contrary to the well stained digital flexors in the forelimb, the mostly unstained parts of the biceps brachii muscle in the upper forelimb still absorbed fresh stain but the final grayscale values in these regions were also significantly lower after the long storage (t-test, $p = 0.012$).

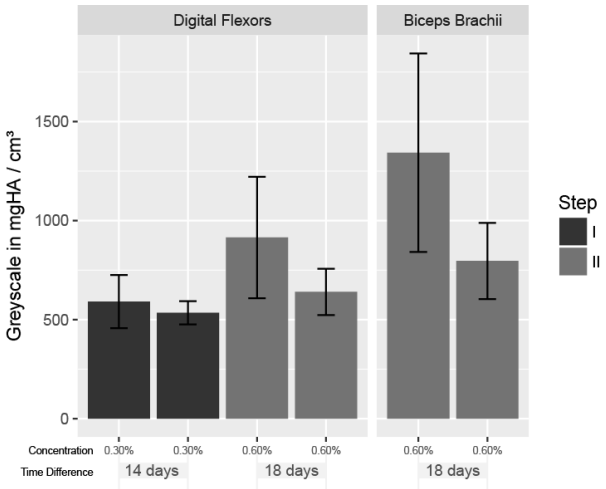

Figure 5: Effect of storage time on muscle tissue staining result; Shown are the grayscale values of the digital flexors and the biceps brachii in the forelimb for the short and long storage time groups at staining steps I (first staining with 0.3%) and II (restained with 0.6%); The 18 day difference in step II resulted in significantly lower grayscale values in both the digital flexors ($p = 0.033$) and the biceps brachii ($p = 0.012$); n = 8 ±SD

Shrinkage is tissue and concentration dependent

As observed by Buytaert et. al.[24], tissue shrinkage does occur in soft tissue with iodine staining at higher concentrations. The overall size of the mouse limbs remained the same in our experiments, there was however a widening of the gaps between muscle fascicles and between muscle and other tissues (Figure 6). While individual tissues shrink, the bone provides a rigid support for the soft tissue and thus prevents a size reduction of the whole sample[25].

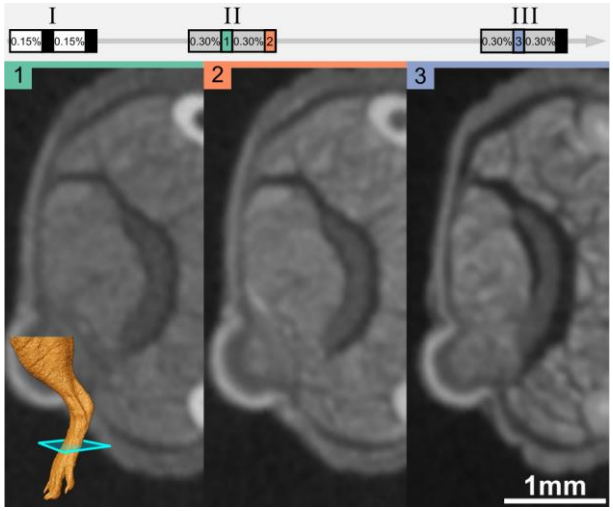

Figure 6: With progressive shrinkage, gaps appear between the muscle fascicles and between different tissues. (1) Staining with 2*0.15% + 1*0.3%: clear gabs between muscles and the tendon, no obvious gaps between fascicles. (2) Staining with 2*0.15% + 2*0.3%: expanded gaps between muscles and tendon. (3) Staining with 2*0.15% + 3*0.3%: gaps between muscles, tendon and skin even wider, gaps between fascicles more pronounced.

Separated organ samples were stained the same way as the hind limbs to determine the shrinkage in different tissue types. With the exception of tendon, which does not appear to shrink due to staining with Lugol's solution, all tissues shrunk considerably (5-25% change in volume) when being placed in 0.15% Lugol's solution over a period of 72h (Figure 7). Shrinkage got progressively more severe with consecutive staining iterations (15-43% change in volume after the final staining).

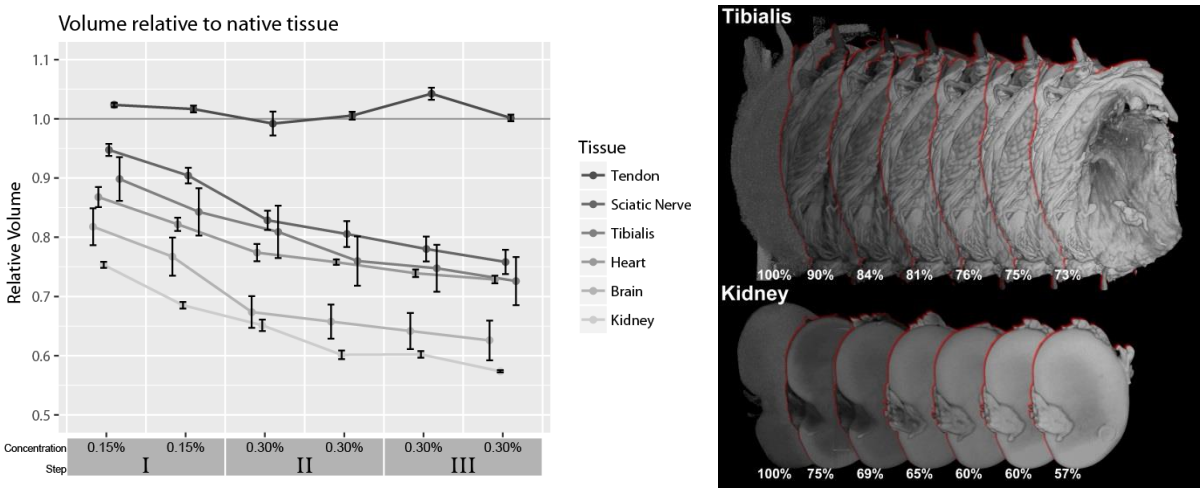

Figure 7: Soft tissue shrinkage at increasing concentrations. Considerable shrinkage already occurs when the samples are initially placed in 0.15% Lugol's solution. Shrinkage increases with consecutive staining

iterations. On the right, volume rendering of µCT images of tibialis and kidney before staining and after each staining step. Percentage values are relative to the volume of the unstained tissue

Staining homogeneity

With low concentrations or a too short staining period, the iodine does not penetrate all the way into the tissue. This results in a stronger staining of the surface of samples. Bone is less permeable to the stain and encapsulated volumes such as the marrow space are mostly unstained at lower concentrations. We also observed that the foot was less heavily stained than the upper thigh. Where muscle was directly exposed to the staining solution, it was also more heavily stained than muscle protected by skin.

Since most of the iodine in the staining solution is taken up by the tissue at these low concentrations, it is expected that the amount of stain will be a major contributor to the final greyscale value. The fore limb received slightly less stain than the hind limb (~17 ml/cm^3 vs. ~20 ml/cm^3) which may explain the lower grayscale values in the digital flexors of the fore limb compared to the flexor digitorum of the hind limb.

Decalcification

As previously described acidic stains such as phosphotungstic acid (PTA) can lead to decalcification of bone tissue and soft tissue shrinkage[2]. We also observed significant decalcification as a result of Lugol staining at high concentrations. No decalcification was observed in the hind limbs up to staining step II which included staining up to a concentration of 0.6%. Starting at staining step III, which repeats the staining of step II (Figure 1), the outer surface of the femur and tibia were decalcified. Decalcification appears more severe when the bone is adjacent to more heavily stained tissue. Bone which was exposed directly to the staining solution or when it lies directly below the skin was also more severely decalcified.

Histological verification of nerve regeneration

When staining at a low enough concentration so that the tissues do not get saturated with iodine, the observed gray values depend on the total amount of the stain used. When trying to identify a tissue of interest, the absolute greyscale is thus not a reliable indicator for the type of tissue and different tissues can only be identified by their morphology and in comparison to surrounding tissues. Figure 8 shows a comparison of the histological stainings MSB and Luxol with the corresponding positions in the µCT (Fig. 8-3). The silk fibroin conduit is stained by Lugol and gives high contrast in the µCT scan. In MSB histology the conduit fibers are visible in red. The position of the histological slice can be found in the µCT based on landmark structures visible in both imaging modalities. In higher magnifications (Fig. 8-4), the correspondence between histology and µCT is apparent. Barium sulfate contrast agent visible in the histology results in a high attenuation in the µCT scan accordingly (A). A large blood vessel which was not perfused with the perfusion contrast agent is visible because of its low attenuation (B). When perfusion does not succeed, the unfilled vessels are completely invisible in the µCT without Lugol's staining. In this regard Lugol's staining can provide a valuable backup for evaluation of blood vessels. Axonal regeneration is visible in the center of the graft (C). The myelin of the regenerating nerve, visible in the Luxol stained histology in blue, absorbs more iodine then the surrounding tissue making it also visible in the µCT. On the maximum intensity projection (3), the position of the histology is shown in yellow. The contrast agent perfused blood vessel (A) is also visible here and can be followed in 3D. It can be shown that this blood vessel originates on the outer surface of the graft. It then penetrates the graft proximal to the position of the

histological slide and continues in a distal direction where it crosses the position of the histological slide. The myelinated axons (C) can also be followed allowing the regeneration front to be identified in 3D. On the minimum intensity projection (4) the blood vessel without perfusion contrast agent (B) can be followed from its proximal origin across the whole graft.

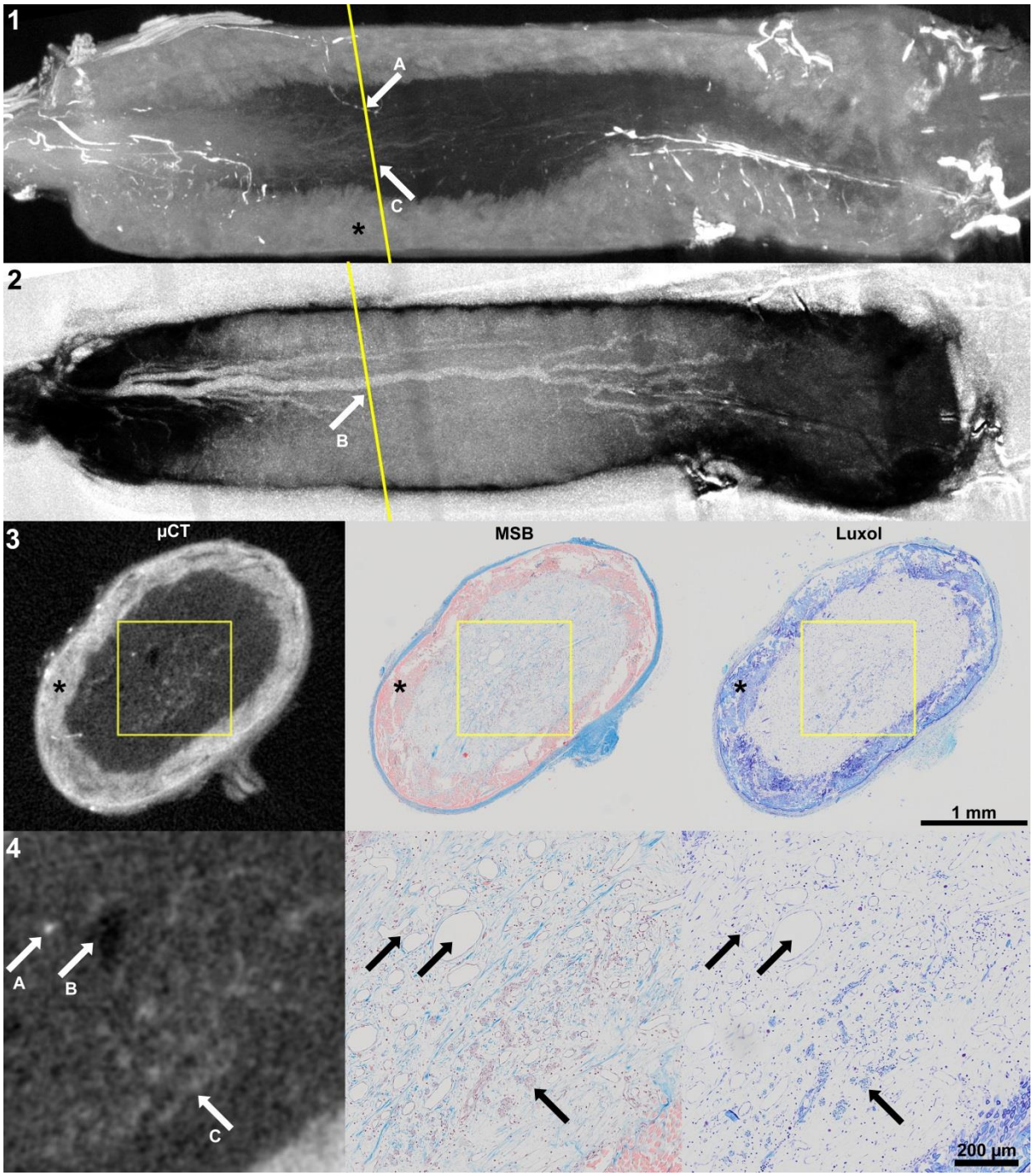

Figure 8: Comparison of µCT with histology work up of a regenerating peripheral nerve in a silk fibroin conduit (asterisk), (1) maximum intensity projection showing the 3D context of perfused blood vessel (A) and regenerated axons (C), (2) inverted minimum intensity projection visualizes bridging of the defect by blood vessel without perfusion with contrast agent (B); (3) Position of the histological slide can be found in µCT due to landmark structures, such as blood vessels contrast agent perfused blood vessels (A), blood vessels without contrast agent (B) and myelinated axons (C) can be identified in histology and µCT, Arrows A,B and C indicate the used landmark structure of the regenerated tissues

Discussion

In contrast to hard tissue regeneration, which can easily be investigated by CT based imaging, the field of soft tissue regeneration lacks a high resolution 3D imaging method. For the analysis of soft tissue regeneration by µCT the main technical requirement is a reliable staining of the tissue of interest while minimizing deleterious influences on the morphology of the tissue. We could show that a good contrast between different tissues can be achieved at different iodine concentrations and while higher concentrations stain tissue quicker, the contrast between tissues remains mostly the same with the amounts of stain used. A longer storage time before staining does appear to reduce the uptake of stain into the tissue (Figure 5). The hind limbs were also stored a comparable time to the forelimbs between staining steps with no obvious negative effects without any apparent loss in contrast between tissues (Figure 4). This suggests that consistency is a more important factor in producing comparable stains than the absolute storage time. Nonetheless, when comparing different samples, we would advise to keep any delays as short as possible and the same for all samples to minimize any possible impact on the staining result.

The final grayscale value in the tissue is determined by the amount of iodine absorbed by the tissue. Since, at the concentrations used, almost all of the iodine is absorbed by the tissue so not only the concentration but also the absolute amount of stain has to be considered. We selected fore- and hindlimbs because they not only have a very consistent size, they also have a range of different tissue types at almost identical relative volume. When planning staining of a tissue sample, the total volume and the relative volume as well as the different affinity towards the stain influence the staining result. Considering that the exact makeup of the sample is often unknown, planning the correct staining amount can therefore be challenging.

We have observed that tissue shrinkage is increased at higher amounts of stain (Figure 7). Since the volume of the organ samples decreases between TP1 & TP2, TP3 & TP4 and TP5 & TP6, which are stained at the same concentrations respectively, the shrinkage appears to be dependent on the total amount of iodine in the tissue, rather than the concentration of the staining solution. Shrinkage appears to be unavoidable, considering that considerable shrinkage occurs already in the first staining step which contains too little iodine to fully stain any of the organ samples with the exception of the sciatic nerves. Similar results were observed by Vickerton et. al. at higher iodine concentrations (2-20%), also recommending using the lowest amount of stain necessary to achieve good contrast. Unfortunately, they do not provide the total amount of staining solution used or whether it was adjusted to the sample volume.[26] To completely avoid shrinkage, other stains such as Hafnium-based Wells-Dawson polyoxometalate (Hf-POM) can be considered which does not appear to result in any shrinkage[27] and was shown to be a promising contrast agent for measurements in soft tissue in µCT[28].

Decalcification only appeared at staining Stage III (corresponds to a cumulative amount of 1*0.3%+2*0.6% or 2*0.15%+4*0.3% respectively), at which point the bone had been exposed to the stain for 60 days. No decalcification was observed in the foot, where the staining appears generally less intense than in the calf or thigh. In the fore limbs, decalcification also occurred despite the lower concentrated Lugol´s solution. This suggests that decalcification increases in severity with longer staining times. The decalcifying effects of Lugol staining are rarely discussed in the literature. Gignac et. al.[29] adapts Lugol staining to larger samples, requiring

longer staining (up to 4 weeks) in higher concentration (11.25%) then commonly used previously, yet does not mention decalcification. Sayin et. al.[30] analyzed the decalcifying effects of 2% Lugol's solution as an endodontic irrigant and found a significant increase of Ca^{2+} ions when exposing the dentin of a human root canal to the Lugol's solution compared to distilled water, thus confirming the decalcifying properties. The decalcifying effect of Lugol's solution appears to be relatively minor even compared to other endodontic irrigants, exhibiting a Ca^{2+} release about four times lower than 2.5% NaOCl[30], the decalcifying properties of which have previously been shown in a similar setup to be almost an order of magnitude lower than 15% ethylenediaminetetraacetic acid (EDTA)[31]. Lugol staining is usually employed to make non-calcified tissues visible in the µCT which, combined with the relatively minor decalcifying effect, may explain why the decalcification is so rarely observed and discussed. However, if calcified structures are of interest, the decalcifying effect of Lugol's solution should be considered.

Tissue penetration is faster at higher concentrations. A short staining time is desirable both for a quicker turnover but also to minimize negative effects such as shrinkage and decalcification of the bone tissue. On the other hand, higher concentrations which shorten the staining time also lead to an increase in tissue shrinkage. For anatomical applications several studies exist where staining parameters are suggested many of which are listed in Gignac *et al.*[4]. However for tissue regeneration purposes where the makeup of the tissue differs strongly from the physiological case and can be further complicated by the presence of non-site-specific materials such as tissue grafts or synthetic implants, such references can provide only limited help. To find the ideal parameters, individual testing appears unavoidable.

Overstaining the tissue increases the negative effects of the staining and should be avoided. We have however shown that applying lower concentrations in multiple steps can result in a very similar outcome than staining in a single high-concentration step. So even if preliminary experiments to optimize the staining are not providing the desired result immediately, a good result can still be achieved with a stepwise staining while avoiding overstaining. Li et. al.[32] suggests a stepwise staining approach with increasing concentrations to preserve a similar concentration difference between the staining solution and the tissue. They observed a more homogenous distribution of stain to the tissue with less shrinkage compared to staining in a single step but with an increased staining duration using their stepwise staining approach.[32]

In anatomical studies, different tissues can often be identified by their location and morphology[2]. When the nature of a tissue is uncertain, correlative histological verification can be used to directly compare the same site with a histological image where the tissue can be clearly identified[33]. In the field of tissue regeneration, where new tissue grows, a proper identification of the tissues of interest is crucial. In case of the sciatic nerve grafts, we could show that regenerating nerve fibers can be identified in the µCT scans. This was confirmed by registering the scans with the histological images allowing for a direct comparison. The Lugol staining had no apparent detrimental impact on the subsequent histological work-up and histological stainings as can be seen in the MSB and Luxol staining (Figure 8). In the study for which the sciatic nerve defects were scanned, the penetration of blood vessels through the silk graft was of interest. With the combination of barium sulfate perfusion and Lugol staining we could locate blood vessel penetrating the graft. The staining also proved useful for verifying whether or not the defect was fully bridged on samples where the longitudinal cuts missed the center of the regenerating nerve. The correlative imaging approach can aid in an improved understanding of the regeneration processes by providing a valuable 3D context to the

histological analysis. The µCT scans can also be used to identify potential sites of interest so that histological sectioning is done at the most interesting positions in the sample.

We believe that the usage of contrast enhanced soft tissue µCT and its 3D information is able to provide novel insights in a variety of fields. In parallel to regeneration of peripheral nervous tissue shown in this study, events after central nervous injuries such as spinal cord injury or brain injury could be analyzed.

Conclusion

Here we present evidence that Lugol staining can provide valuable additional information for understanding tissue regeneration processes. We discuss potential pitfalls of contrast enhanced soft tissue µCT imaging and provide solutions for the usage of Lugol´s solution. We consider individual adjustments to the staining process to be necessary for staining different tissues. Incremental staining can help ease the optimization process, reduce the risk of overstaining and help minimize shrinkage associated with higher concentrations. In this work we are the first to visualize regenerating nervous tissue using contrast enhanced µCT. One of the major advantages of this imaging method is the possibility to identify and preselect sites of interest for subsequent histological sectioning using µCT analysis. Histologic techniques can be used to verify structures visible in the µCT to reduce the risk of misidentifying tissues while the µCT can provide valuable 3D context to histological observations. Correlative imaging of Lugol stained µCT and conventional histology can mutually improve the interpretation in both imaging techniques.

Data availability

Original µCT data of the hind limbs, fore limbs and organ samples can be made available upon request to the corresponding author.

Conflicts of Interest

None.

Funding Statement

The authors received no specific funding for this work.

Author Contributions

PH, NS, PS, MK, DH, HR participated in the study design. PH, NS, MK, DH Conducted the study. NS, MK, DH performed the surgeries. AT developed and provided the nerve grafts. PH, NS performed µCT scanning. SN performed histology. PH performed the data analysis and wrote the manuscript. PH, AT, DH, PS participated in the data interpretation. PS, HR, AT, DH aided in the review process and provided scientific input.

References

1. Dimitriou, R., Jones, E., McGonagle, D. & Giannoudis, P. V. Bone regeneration: current concepts and future directions. *BMC Med.* **9,** 66 (2011).
2. Metscher, B. D. MicroCT for developmental biology: A versatile tool for high-contrast 3D imaging at histological resolutions. *Dev. Dyn.* **238,** 632–640 (2009).
3. Metscher, B. D. MicroCT for comparative morphology: simple staining methods allow high-contrast 3D imaging of diverse non-mineralized animal tissues. *BMC Physiol.* **9,** 11 (2009).
4. Gignac, P. M. *et al.* Diffusible iodine-based contrast-enhanced computed tomography (diceCT): an emerging tool for rapid, high-resolution, 3-D imaging of metazoan soft tissues. *J. Anat.* **228,** 889–909 (2016).
5. Lafage-Proust, M.-H. *et al.* Assessment of bone vascularization and its role in bone remodeling. *BoneKEy Rep.* **4,** 662 (2015).
6. Blery, P. *et al.* Vascular imaging with contrast agent in hard and soft tissues using microcomputed-tomography. *J. Microsc.* **262,** 40–49 (2016).
7. Kingston, M. J., Perriman, D. M., Neeman, T., Smith, P. N. & Webb, A. L. Contrast agent comparison for three-dimensional micro-CT angiography: A cadaveric study. *Contrast Media Mol. Imaging* **11,** 319–324 (2016).
8. Evans, G. R. Challenges to nerve regeneration. *Semin. Surg. Oncol.* **19,** 312–318 (2000).
9. Lee, S. K. & Wolfe, S. W. Peripheral nerve injury and repair. *J. Am. Acad. Orthop. Surg.* **8,** 243–252 (2000).
10. Nectow, A. R., Marra, K. G. & Kaplan, D. L. Biomaterials for the Development of Peripheral Nerve Guidance Conduits. *Tissue Eng. Part B Rev.* **18,** 40–50 (2011).
11. Millesi, H. Bridging defects: autologous nerve grafts. in *How to Improve the Results of Peripheral Nerve Surgery* 37–38 (Springer, Vienna, 2007). doi:10.1007/978-3-211-72958-8_8
12. Best, T. J., Mackinnon, S. E., Midha, R., Hunter, D. A. & Evans, P. J. Revascularization of peripheral nerve autografts and allografts. *Plast. Reconstr. Surg.* **104,** 152–160 (1999).

13. Farber, S. J. *et al.* Vascularization is delayed in long nerve constructs compared to nerve grafts. *Muscle Nerve* **54,** 319–321 (2016).

14. Yu, D.-Z. *et al.* Two methods can simultaneously display both intramuscular nerves and blood vessels. *Plast. Reconstr. Surg.* **129,** 401–411 (2012).

15. Sihler, C. Ueber Muskelspindeln und intramuskuläre Nervenendigungen bei Schlangen und Fröschen. *Arch. Für Mikrosk. Anat.* **46,** 709–723 (1895).

16. Gülekon, N., Peker, T., Turgut, H. B., Anıl, A. & Karaköse, M. Qualitative comparison of anatomical microdissection, Sihler's staining and computerized reconstruction methods for visualizing intramuscular nerve branches. *Surg. Radiol. Anat.* **29,** 373–378 (2007).

17. Teuschl, A. H. *et al.* A New Preparation Method for Anisotropic Silk Fibroin Nerve Guidance Conduits and Its Evaluation In Vitro and in a Rat Sciatic Nerve Defect Model. *Tissue Eng. Part C Methods* **21,** 945–957 (2015).

18. Teuschl, A. H., van Griensven, M. & Redl, H. Sericin removal from raw Bombyx mori silk scaffolds of high hierarchical order. *Tissue Eng. Part C Methods* **20,** 431–439 (2014).

19. Schneider, C. A., Rasband, W. S. & Eliceiri, K. W. NIH Image to ImageJ: 25 years of image analysis., NIH Image to ImageJ: 25 years of Image Analysis. *Nat. Methods Nat. Methods* **9, 9,** 671, 671–675 (2012).

20. Schindelin, J. *et al.* Fiji: an open-source platform for biological-image analysis. *Nat. Methods* **9,** 676–682 (2012).

21. Hoffman, E. J., Huang, S. C. & Phelps, M. E. Quantitation in positron emission computed tomography: 1. Effect of object size. *J. Comput. Assist. Tomogr.* **3,** 299–308 (1979).

22. R Core Team. R: A language and environment for statistical computing. (2017).

23. Wickham, H. *ggplot2: Elegant Graphics for Data Analysis*. (Springer-Verlag).

24. Buytaert, J., Goyens, J., Greef, D. D., Aerts, P. & Dirckx, J. Volume Shrinkage of Bone, Brain and Muscle Tissue in Sample Preparation for Micro-CT and Light Sheet Fluorescence Microscopy (LSFM). *Microsc. Microanal.* **20,** 1208–1217 (2014).

25. Li, Z., Ketcham, R. A., Yan, F., Maisano, J. A. & Clarke, J. A. Comparison and Evaluation of the Effectiveness of Two Approaches of Diffusible Iodine-Based Contrast-Enhanced Computed Tomography (diceCT) for Avian Cephalic Material. *J. Exp. Zoolog. B Mol. Dev. Evol.* **326,** 352–362 (2016).

26. Vickerton, P., Jarvis, J. & Jeffery, N. Concentration-dependent specimen shrinkage in iodine-enhanced microCT. *J. Anat.* **223,** 185–193 (2013).

27. Kerckhofs, G. *et al.* Novel non-invasive contrast agents for virtual histology and 3D quantification of soft tissues. in *User Meeting Bruker MicroCT* (2016).

28. Kerckhofs, G. *et al.* Simultaneous three-dimensional visualization of mineralized and soft skeletal tissues by a novel microCT contrast agent with polyoxometalate structure. *Biomaterials* **159,** 1–12 (2018).

29. Gignac, P. M. & Kley, N. J. Iodine-enhanced micro-CT imaging: methodological refinements for the study of the soft-tissue anatomy of post-embryonic vertebrates. *J. Exp. Zoolog. B Mol. Dev. Evol.* **322,** 166–176 (2014).

30. Sayin, T. C. *et al.* Time-dependent Decalcifying Effects of Endodontic Irrigants with Antibacterial Properties. *J. Endod.* **35,** 280–283 (2009).

31. Pérez-Heredia, M., Ferrer-Luque, C. M., González-Rodríguez, M. P., Martín-Peinado, F. J. & González-López, S. Decalcifying effect of 15% EDTA, 15% citric acid, 5% phosphoric acid and 2.5% sodium hypochlorite on root canal dentine. *Int. Endod. J.* **41,** 418–423 (2008).

32. Li, Z., Clarke, J. A., Ketcham, R. A., Colbert, M. W. & Yan, F. An investigation of the efficacy and mechanism of contrast-enhanced X-ray Computed Tomography utilizing iodine for large specimens through experimental and simulation approaches. *BMC Physiol.* **15,** 5 (2015).

33. Herdina, A. N. *et al.* Correlative 3D-imaging of Pipistrellus penis micromorphology: Validating quantitative microCT images with undecalcified serial ground section histomorphology. *J. Morphol.* **276,** 695–706 (2015).